

## Dispersion and Nonlinearity Identification for Single-Mode Fibers Using the Nonlinear Fourier Transform

De Koster, Pascal; Wahls, Sander

**DOI**

[10.1109/JLT.2020.2979285](https://doi.org/10.1109/JLT.2020.2979285)

**Publication date**

2020

**Document Version**

Final published version

**Published in**

Journal of Lightwave Technology

**Citation (APA)**

De Koster, P., & Wahls, S. (2020). Dispersion and Nonlinearity Identification for Single-Mode Fibers Using the Nonlinear Fourier Transform. *Journal of Lightwave Technology*, 38(12), 3252-3260. <https://doi.org/10.1109/JLT.2020.2979285>

**Important note**

To cite this publication, please use the final published version (if applicable). Please check the document version above.

**Copyright**

Other than for strictly personal use, it is not permitted to download, forward or distribute the text or part of it, without the consent of the author(s) and/or copyright holder(s), unless the work is under an open content license such as Creative Commons.

**Takedown policy**

Please contact us and provide details if you believe this document breaches copyrights. We will remove access to the work immediately and investigate your claim.

# Dispersion and Nonlinearity Identification for Single-Mode Fibers Using the Nonlinear Fourier Transform

Pascal de Koster<sup>1</sup> and Sander Wahls<sup>1</sup>, *Senior Member, IEEE*

**Abstract**—Efficient fiber-optic communication requires precise knowledge of the fiber coefficients, but these often change over time due to factors such as aging or bending. We propose a novel algorithm that identifies the average second-order dispersion and Kerr nonlinearity coefficient of a fiber, without employing any special training signals. Instead, ordinary input and output data recorded during normal operation is used. To the best of our knowledge, this is the first such algorithm. The algorithm is based on the nonlinear Fourier spectrum of the signal, which is known to evolve trivially as the signal propagates through an idealized model of the fiber. The algorithm varies the values of the fiber coefficients until the corresponding nonlinear Fourier spectrum at transmitter and receiver match optimally. We test the algorithm on simulated transmission data over a 1600 km link, and accurately identify the fiber coefficients. The identification algorithm is in particular well suited for providing a fiber model for nonlinear Fourier transform-based communication.

**Index Terms**—Chromatic dispersion, digital signal processing, fiber identification, fiber-optic communications, Kerr nonlinear effect, nonlinear Fourier transform.

## I. INTRODUCTION

DIGITAL signal processing has become increasingly more important in fiber-optic communication systems with high data rates, as it allows to compensate for transmission impairments such as chromatic dispersion and the Kerr nonlinear effect [1]–[3]. In order to digitally compensate such effects, the fiber is often modelled with a lossy and noisy nonlinear Schrödinger equation, in which the second-order dispersion coefficient  $\beta_2$  and the Kerr nonlinearity coefficient  $\gamma$  are assumed to be known. The values of these two coefficients are usually supplied by the manufacturer of the fiber link, but it often occurs that the supplied values do not exactly fit the fiber anymore after installation of the fiber due to bending, aging, and splicing [1]. It may also occur that the fiber coefficients are not readily available, or lost, as may be the case in small scale experimental setups. For such scenarios, we present a novel nonlinear Fourier transform (NFT)-based fiber identification algorithm to determine the

values of  $\beta_2$  and  $\gamma$ , using input-output transmission data only. This paper improves and extends our earlier NFT-based fiber identification algorithm [4] in terms of robustness, versatility and accuracy.

Several fiber identification algorithms have already been developed, but these either identify only  $\beta_2$  (e.g., [5], [6]), or identify  $\gamma$  using digital back-propagation (e.g., [7]–[10]). However, these algorithms using digital back-propagation suffer from at least one of the following shortcomings:  $\beta_2$  has to be known; a specific modulation format has to be used; the quality of the estimates depends on the chosen spatial numerical step. Other methods determine  $\gamma$  by measuring self-phase modulation, cross-phase modulation, or four-wave mixing using training signals [11]–[13], but these require that normal operation of the fiber is interrupted, which can be undesirable in scenarios where the system is in constant operation, or when the training signals are not straight-forward to generate or analyze. Furthermore, several of these identification algorithms were demonstrated for short fibers, and may therefore be less suitable for identifying long links. Finally, we remark that applying standard black-box machine learning techniques for fiber parameter identification is not straight-forward. Due to their black-box nature, known physical models are not exploited. Instead, one has to provide large representative data sets that cover a wide range of real-world scenarios, which is a challenging problem in itself.

To overcome these drawbacks of current identification methods, we present a novel algorithm that identifies average values for both  $\beta_2$  and  $\gamma$ , by comparing the nonlinear Fourier spectrum of transmitted and received signals. Theory predicts that the NFT spectrum at the transmitter and the NFT spectrum at the receiver are linearly related for a noiseless lossless link [14]. Since additional loss and noise effects occurring in realistic links can be taken into account using proper transformations, it is possible to use the NFT spectrum for identification.

The NFT is typically computed with respect to a normalized nonlinear Schrödinger equation (NLSE), which requires the provided input-output data to be normalized. Our algorithm uses the fact that the NFT spectrum at input and output only match if the input and output signal are normalized with the correct amplitude normalization constant  $c_q$  and normalized fiber length  $Z$ , which both depend on  $\beta_2$  and  $\gamma$ . First, an initial estimate for  $c_q$  is determined by comparing the third conserved quantities of the NLSE of the input and output signals [15]. Starting from this initial guess,  $c_q$  is varied first and then  $Z$  until we find the

Manuscript received December 20, 2019; revised February 14, 2020; accepted March 3, 2020. Date of publication March 9, 2020; date of current version June 16, 2020. (Corresponding author: Pascal de Koster.)

The authors are with the Delft Center for System and Control, Delft University of Technology 2628 CD, Delft, The Netherlands (e-mail: p.b.j.dekoster@tudelft.nl; s.wahls@tudelft.nl).

Color versions of one or more of the figures in this article are available online at <http://ieeexplore.ieee.org>.

Digital Object Identifier 10.1109/JLT.2020.2979285

normalization at which the NFT spectrum at input and output match optimally. Assuming that the attenuation, fiber length, and amplifier spacing are known, we can derive  $\beta_2$  and  $\gamma$  from the identified normalization  $c_q$  and  $Z$ .

Another application of our proposed algorithm is the identification of a suitable model for NFT-based communication systems [16], without any prior knowledge of the fiber. NFT-based transmission systems typically only require the correct normalization constant  $c_q$  and normalized length  $Z$ , and can therefore be calibrated, even if no information of the fiber link is available at all.

This paper is structured as follows. Section II gives an overview of the fiber model and the nonlinear Fourier transform. Section III provides two identification algorithms, based on the continuous NFT spectrum and the discrete NFT spectrum, respectively. Section IV combines both algorithms into one final robust algorithm. Section V evaluates the final algorithm with simulated test cases and Section VI concludes the paper.

## II. FIBER MODEL AND NONLINEAR FOURIER TRANSFORM

The propagation of light through an optical single-mode fiber under the influence of anomalous dispersion, self-focusing, attenuation, lumped amplification, and noise can be modelled by the focusing nonlinear Schrödinger equation [1, Ch. 9.1.1]:

$$A_l = -i\frac{\beta_2}{2}A_{\tau\tau} + i\gamma|A|^2A - \frac{\alpha}{2}A + \sum_{n=1}^N (rA + G(r, n))\delta(l - nL_{\text{span}}), \quad (1)$$

in which  $\tau$  denotes retarded time,  $l$  the position in the fiber,  $A(\tau, l)$  the complex field envelope,  $\beta_2 < 0$  the dispersion coefficient,  $\gamma$  the Kerr nonlinearity coefficient,  $\alpha$  the attenuation coefficient,  $i$  the unit imaginary number, and  $\delta$  the Dirac delta function. Subscripts indicate partial derivatives. The link of length  $L$  consists of  $N$  equidistant fiber spans, each with length  $L_{\text{span}} = L/N$ . At the end of each span,  $l = nL_{\text{span}}$ , an Erbium Doped Fiber Amplifier (EDFA) is used to amplify the signal with a factor  $r = e^{\alpha L_{\text{span}}/2}$  (lumped amplification) to compensate the loss. Additive white Gaussian noise  $G(r, n)$  enters the system through Amplified Spontaneous Emission (ASE) during amplification, with noise power dependent on the noise figure of the EDFA and the amplification factor  $r$ .

Within each fiber span, the amplifiers can be ignored, and we may change to the variable  $Q(\tau, l) = e^{\alpha l/2}A(\tau, l)$ , which yields a lossless NLSE with varying Kerr effect:

$$Q_l = -i\frac{\beta_2}{2}Q_{\tau\tau} + i\gamma e^{-\alpha l}|Q|^2Q. \quad (2)$$

Assuming that the wave envelope does not change much within each fiber span, we may approximate Eq. 2 with a lossless path-averaged (LPA) NLSE [17], in which the varying nonlinearity coefficient is approximated with its path average,  $\gamma_1$ . This leads to the LPA-NLSE:

$$\gamma_1 = \frac{1}{L_{\text{span}}} \int_0^{L_{\text{span}}} \gamma e^{-\alpha l} dl = \gamma \frac{1 - e^{-\alpha L_{\text{span}}}}{\alpha L_{\text{span}}}, \quad (3)$$

$$Q_l \approx -i\frac{\beta_2}{2}Q_{\tau\tau} + i\gamma_1|Q|^2Q. \quad (4)$$

When distributed Raman amplification is applied instead of lumped amplification, path averaging can also be applied using an integral with  $l$ -dependent attenuation. A link with distributed Raman amplification is typically approximated better by the LPA-NLSE than a similar link with lumped amplification [18]. In this paper, we therefore focus on the more challenging case of lumped amplification.

The proposed fiber identification algorithm in this paper is based on comparing the NFT of input and output signals, for which the NLSE is required in normalized form. Let  $T_0$  be a free time scaling parameter. We will only consider  $T_0 = 1$  s for the identification algorithm, as increasing  $T_0$  only linearly scales the nonlinear frequency  $\lambda$  in the NFT. We then switch to the normalized variables [19]

$$t = \frac{1}{T_0} \tau, \quad q = T_0 \underbrace{\sqrt{\frac{\gamma_1}{-\beta_2}}}_{c_q} Q, \quad z = \frac{1}{T_0^2} \underbrace{\frac{-\beta_2}{2}}_{c_z} l, \quad (5)$$

This results in the normalized NLSE:

$$q_z = iq_{tt} + 2i|q|^2q. \quad (6)$$

Note that  $\beta_2$  appears in the denominator of  $c_q$ . Small mismatches in  $\beta_2$  might therefore result in large changes in the normalized signal  $q$ . Hence, the proposed NFT-based identification algorithm may be less suited for dispersion managed links with near-zero average dispersion.

The normalized NLSE may be solved exactly in the nonlinear Fourier domain, in which the NFT spectrum of the signal evolves trivially. The NFT of a signal  $q(t)$  can be determined by solving the Zakharov-Shabat scattering problem [14], [15]:

$$\frac{d}{dt} \begin{bmatrix} \phi_1(t, \lambda) \\ \phi_2(t, \lambda) \end{bmatrix} = \begin{bmatrix} -i\lambda & q(t) \\ -q^*(t) & i\lambda \end{bmatrix} \begin{bmatrix} \phi_1(t, \lambda) \\ \phi_2(t, \lambda) \end{bmatrix},$$

$$\begin{bmatrix} \phi_1(t, \lambda) \\ \phi_2(t, \lambda) \end{bmatrix} \xrightarrow{t \rightarrow +\infty} \begin{bmatrix} e^{-i\lambda t} \\ 0 \end{bmatrix}, \quad (7)$$

where  $(\cdot)^*$  denotes the complex conjugate. We then define the scattering coefficients  $a(\lambda)$  and  $b(\lambda)$  as the normalized limits of  $\phi_1$  and  $\phi_2$  for  $t \rightarrow +\infty$ :

$$a(\lambda) := \lim_{t \rightarrow +\infty} e^{i\lambda t} \phi_1(t, \lambda), \quad b(\lambda) := \lim_{t \rightarrow +\infty} e^{-i\lambda t} \phi_2(t, \lambda). \quad (8)$$

The NFT of  $q(t)$  consists of a continuous and a discrete spectrum. We define the continuous spectrum as  $b(\lambda)$ ,  $\lambda \in \mathbb{R}$ , and the discrete spectrum as  $\{\lambda_m, b_m\}_{m=1}^M$ , in which the eigenvalues  $\lambda_m$  are the zeros of  $a(\lambda)$  in the complex upper half plane, and  $b_m = b(\lambda_m)$ . Each eigenvalue  $\lambda_m$  in the discrete spectrum corresponds to a *solitonic component* in the signal, a shape-retaining, localized wave. The continuous spectrum represents dispersive components. As the signal  $q(t, z)$  propagates in the  $z$ -direction according to the normalized NLSE (6), the eigenvalues remain invariant, while the scattering coefficients evolve trivially [14]:

$$a(\lambda, z) = a(\lambda, 0), \quad b(\lambda, z) = b(\lambda, 0)e^{4i\lambda^2 z}. \quad (9)$$

### III. IDENTIFICATION USING ONLY CONTINUOUS OR DISCRETE SPECTRUM

In this section, we present two separately executable algorithms to estimate the fiber coefficients, which are combined into one robust, final algorithm in Section IV. Both algorithms are based on the simple evolution of the scattering coefficients in Eq. 9. The first algorithm takes only the continuous spectrum into account; the second algorithm considers only the discrete spectrum. Both algorithms can be split into two separate single-parameter identification problems: first, the amplitude normalization  $c_q = \sqrt{\gamma_1/(-\beta_2)}$  is identified, and second, the normalized link length  $Z := c_z L = -\frac{\beta_2}{2} L$ . The amplitude normalization will be determined using a local optimization technique, starting from an initial guess. The third integral of motion of the normalized NLSE can be used to obtain an initial estimate,  $c_q^0$ , as described in the Appendix. If other prior knowledge is available of the fiber, this may also be taken into account for the initialization.

For the proposed algorithm, we have chosen to define the NFT spectrum as  $b(\lambda)$ , although it is also common to define the continuous spectrum as  $\hat{q}(\lambda) := b/a$ ,  $\lambda \in \mathbb{R}$ , and the discrete spectrum as  $\{\lambda_m, \tilde{q}_m\}_{m=1}^M$ , with  $\tilde{q}_m := b/a_\lambda(\lambda_m)$  (i.e., the residue of  $\hat{q}$  in  $\lambda_m$ ). We have chosen to use only  $b(\lambda)$ , as it is usually less noisy than  $b(\lambda)/a(\lambda)$ , (see e.g., [20]).

#### A. Identification From the Continuous NFT Spectrum

The first identification algorithm considers only the continuous part of the NFT,  $b(\lambda)$ ,  $\lambda \in \mathbb{R}$ . Note that the nonlinear Fourier transform of a signal depends on the applied amplitude normalization,  $c_q$ , in Eq. 5. We denote the  $b$ -coefficient in (8) that corresponds to the signal  $q(t) = T_0 c_q Q(T_0 t)$  in (7) by  $b(\lambda, z; c_q)$ , where  $z$  denotes the normalized position of  $Q$  in the fiber.

We observe from Eq. 9 that the correct value  $c_q = c_q^*$  leads to a constant absolute value of  $|b|$  throughout an ideal fiber, and in particular, the absolute value at input ( $z = 0$ ) and at output ( $z = Z/T_0^2$ ) are equal:

$$|b(\lambda, Z/T_0^2; c_q^*)| = |b(\lambda, 0; c_q^*)|, \quad \lambda \in \mathbb{R}. \quad (10)$$

We may substitute  $b^{\text{in}}(\lambda; c_q) = b(\lambda, 0; c_q)$  and  $b^{\text{out}}(\lambda; c_q) = b(\lambda, Z/T_0^2; c_q)$ , which are determined from the NFT of the normalized transmitted signal  $q^{\text{in}}(t)$  and received signal  $q^{\text{out}}(t)$  respectively. Our strategy will be to vary  $c_q$ , and identify the normalization for which the  $|b|$  of the transmitted and received signal match as well as possible. As shown in Fig. 1, the absolute continuous spectrum at input and output are indeed nearly identical for the optimal amplitude normalization,  $c_q^*$ , whereas a sub-optimal  $c_q$  may cause a significant mismatch.

To quantify the mismatch, we measure the normalized absolute error over a range of nonlinear frequencies  $[\lambda_{\min}, \lambda_{\max}]$ :

$$E_{|\text{cs}|}(c_q) = \frac{\int_{\lambda_{\min}}^{\lambda_{\max}} ||b^{\text{out}}(\lambda; c_q)| - |b^{\text{in}}(\lambda; c_q)|| d\lambda}{\int_{\lambda_{\min}}^{\lambda_{\max}} |b^{\text{in}}(\lambda; c_q)| d\lambda}, \quad (11)$$

in which  $E_{|\text{cs}|}$  denotes the relative error in the absolute value of the continuous spectrum. The error is normalized with the

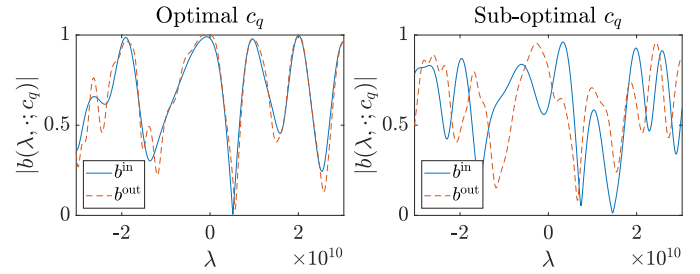


Fig. 1. The absolute continuous spectrum at input and output at optimal  $c_q$  (left), and at sub-optimal  $c_q$  (right).

$b$ -coefficient of the transmitted signal, as it does not contain any ASE-noise, in contrast to the received signal. The range  $[\lambda_{\min}, \lambda_{\max}]$  is determined by considering the occupied bandwidth, i.e., the smallest linear frequency range containing at least (e.g.) 90% of the signal energy:

$$[\lambda_{\min}, \lambda_{\max}] = [-\omega_{\max}/2, -\omega_{\min}/2], \quad \text{such that}$$

$$\int_{\omega_{\min}}^{\omega_{\max}} |\mathcal{F}(q)(\omega)|^2 d\omega \geq 0.9 \int_{-\infty}^{+\infty} |\mathcal{F}(q)(\omega)|^2 d\omega, \quad (12)$$

with  $\mathcal{F}(q)(\omega)$  the linear Fourier transform of  $q(t)$  at angular frequency  $\omega$ . The reason for this choice is that the NFT of an infinitesimal-energy signal  $q(t)$  and the linear Fourier transform of  $q(t)$  relate through [19]

$$b(\lambda) = -(\mathcal{F}(q)(-2\lambda))^*. \quad (13)$$

Also for higher-energy signals, (i.e., when the linear and nonlinear Fourier transform differ significantly), we observed that the frequency range  $[\lambda_{\min}, \lambda_{\max}]$  still contains a significant amount of the energy, leading to a good signal-to-noise ratio for the identification algorithm.

We minimize (11) with respect to  $c_q$  by first performing a coarse line search around the initial guess,  $c_q^0$ . The grid point with minimal error is then used as initial guess for the local minimization scheme from [21] (i.e., the standard *fminsearch* function in *Matlab*) to obtain an estimate  $\hat{c}_q$ .

*Comparing phase shifts to find  $Z$* : After identifying  $c_q$  from  $|b(\lambda)|$ , we may extract the normalized length  $Z$  by comparing the phase shift between the continuous spectrum at receiver and transmitter. From this point on, we consider only  $b(\lambda, z) = b(\lambda, z; \hat{c}_q)$  with  $\hat{c}_q$  identified in the previous step. Assuming propagation through an ideal fiber with  $\hat{c}_q = c_q^*$  and the correct normalized length,  $Z^*$ , the phase shift in  $b(\lambda, z)$  according to (9) is given by

$$\angle b(\lambda, Z^*/T_0^2) = \angle b(\lambda, 0) + 4\lambda^2 Z^*/T_0^2 \pmod{2\pi}, \quad \lambda \in \mathbb{R}. \quad (14)$$

By replacing  $b(\lambda, 0)$  with the determined  $b^{\text{in}}(\lambda)$ , and  $b(\lambda, 0)$  with  $b^{\text{out}}(\lambda)$ , Eq. 14 will hold approximately if  $\hat{c}_q \approx c_q^*$  and  $Z \approx Z^*$ . Note that Eq. 14 corresponds to fitting a parabola  $\lambda^2$  to the phase shift in  $b$ , in a  $2\pi$ -periodic space. When identifying  $Z$ , we will also allow an offset  $\psi_0$  in the parabola.

We first estimate  $Z$  and  $\psi_0$  by fitting  $4\lambda^2 Z/T_0^2 + \psi_0$  with linear least squares to the unwrapped phase difference,  $\Delta\psi(\lambda) := \text{unwrap}(\angle b^{\text{out}} - \angle b^{\text{in}})$ , with  $\Delta\psi(0) \in [-\pi, \pi)$ , and

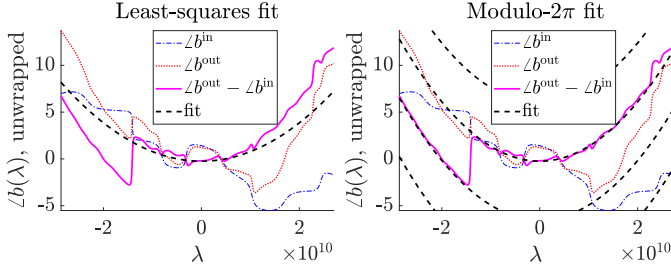


Fig. 2. Left: the initial least squares quadratic fit to the unwrapped phase difference. Right: the quadratic fit to the unwrapped phase difference resulting from (15), which allows for  $2\pi$  phase shifts.

$\lambda \in [\lambda_{\min}, \lambda_{\max}]$ . Although the resulting estimates are usually accurate, it may occur that the phase difference is unwrapped to the wrong side, causing  $2\pi$  jumps in the unwrapped phase difference (see Fig. 2, left). Therefore, we define an error norm that is not affected by these  $2\pi$  jumps:

$$E_{\mathcal{L}_{cs}}(Z, \psi_0) = \frac{1}{\lambda_{\max} - \lambda_{\min}} \int_{\lambda_{\min}}^{\lambda_{\max}} \left| [\mathcal{L}b^{\text{out}}(\lambda) - \mathcal{L}b^{\text{in}}(\lambda) - (4\lambda^2 Z/T_0^2 + \psi_0) + \pi] \bmod 2\pi - \pi \right| d\lambda, \quad (15)$$

in which  $E_{\mathcal{L}_{cs}}$  denotes the average error in the phase of the continuous spectrum. Note that we add  $\pi$  before the modulo operation, and subtract  $\pi$  afterwards to ensure the phase mismatch at every  $\lambda$  is in the region  $[-\pi, \pi)$  instead of  $[0, 2\pi)$ . Similar to the optimization of  $E_{|cs|}$  (11), we first perform a coarse line search around the linear least squares estimate for  $Z$ , and then the iterative minimization scheme from [21] to obtain final estimates  $\hat{Z}$  and  $\hat{\phi}_0$ .

### B. Identification From the Discrete NFT Spectrum

In this subsection, we propose a method to identify the normalization  $c_q$  and normalized length  $Z$  by comparing the discrete spectra of the transmitted and received signal. Similar to the continuous spectrum algorithm, we will first identify  $c_q$ , and  $Z$  afterwards.

We start by writing the discrete spectrum with an explicit dependence on  $c_q$ . We denote the discrete spectrum that corresponds to the signal  $q(t) = T_0 c_q Q(T_0 t)$  by  $\{\lambda_m(c_q), b_m(z; c_q)\}_{m=1}^{M(c_q)}$ , with  $z$  the normalized position of  $Q$  in the fiber. We note here that the energy  $\mathcal{E}_m$  of the solitonic component corresponding to the eigenvalue  $\lambda_m$  increases with its imaginary part,  $\mathcal{E}_m = 4\Im(\lambda_m)$  [19]. Increasing  $c_q$  increases the normalized signal energy, which usually increases energy in the discrete spectrum as well. As a result, on average the eigenvalues meander upwards in the complex plane in continuous trajectories, and new eigenvalues may appear from the real axis [22],[23, p. 12]. For small values of  $c_q$  however, the normalized energy will be too low, and the discrete spectrum will contain no eigenvalues at all [24].

If the correct normalization  $c_q^*$  is applied, the eigenvalues  $\lambda_m$  remain constant, and each  $b(\lambda_m)$  evolves according to (9), assuming a lossless, noiseless fiber. Also for a non-ideal fiber, the

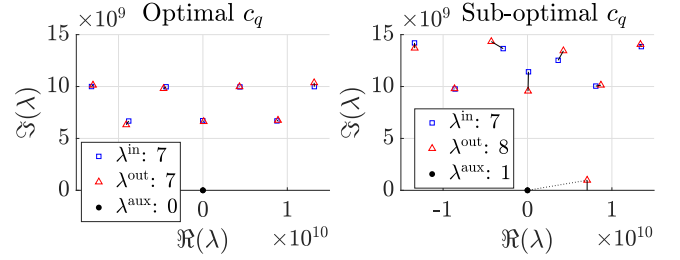


Fig. 3. The eigenvalues of a transmitted 7-soliton signal, evaluated with the optimal normalization  $c_q$  (left), and with a sub-optimal  $c_q$  (right). Connections indicate the least-cost perfect matching.

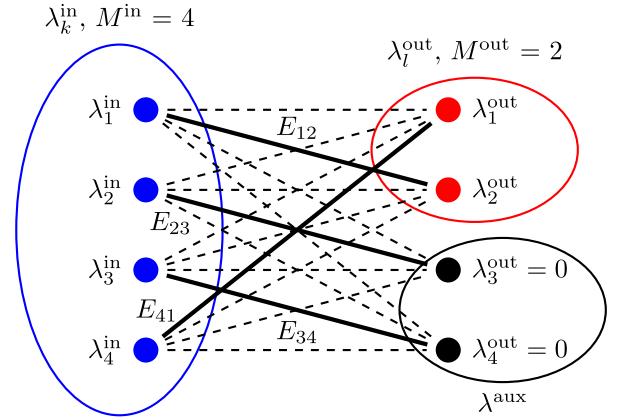


Fig. 4. The complete bipartite graph corresponding to 4 input eigenvalues, and 2 output eigenvalues. 2 auxiliary eigenvalues have been added to the set of output eigenvalues to ensure that the output and input eigenvalue sets are equally large. A possible perfect matching  $l(k)$  is marked:  $\{l(1) = 2, l(2) = 3, l(3) = 4, l(4) = 1\}$ . The cost of this matching is  $E_{12} + E_{23} + E_{34} + E_{41}$ .

solitonic components of the eigenvalues are still preserved relatively well, as long as both the span length is much shorter than the corresponding soliton period [25] and the signal-to-noise ratio is sufficiently high. We will use this property, and identify the normalization  $c_q$  for which the discrete spectrum at transmitter and at receiver correspond as well as possible. To illustrate the effect of the normalization  $c_q$  on the discrete eigenvalues, Fig. 3 shows the spectrum of a 7-soliton signal [26] at both transmitter and receiver. The left eigenvalues were determined with the optimal  $c_q^*$ . The right spectra were determined with a 22% larger  $c_q$ , which caused a larger difference between the spectra compared to the optimal  $c_q$ . We also note that the increase in  $c_q$  resulted in more normalized energy, and accordingly, the eigenvalues have shifted upwards, and a new, unmatched output eigenvalue has spawned from the real axis.

To quantify the error between the input and output spectrum for a given  $c_q$ , we propose an error norm based on creating pairs of eigenvalues at input and output, and sum the error in each pair. Note that the number of input eigenvalues,  $M^{\text{in}}$ , and the number of output eigenvalues,  $M^{\text{out}}$ , may be unequal,  $M^{\text{in}} \neq M^{\text{out}}$ . To allow for a perfect matching, we keep adding ‘auxiliary eigenvalues’ at zero,  $\lambda^{\text{aux}} = 0$ , to the smaller set until the sets are equally large (see also Fig. 3, right). Next, we create a complete bipartite graph as shown in Fig. 4. Each input eigenvalue  $\lambda_k^{\text{in}}$  connects to each output eigenvalue  $\lambda_l^{\text{out}}$  with edges  $(\lambda_k^{\text{in}}, \lambda_l^{\text{out}})$ ,

with associated cost  $E_{kl}$ . The cost of the edges represents the mismatch between eigenvalue  $\lambda_k^{\text{in}}$  and  $\lambda_l^{\text{out}}$ , and will be specified later in this section, but we already mention that each edge cost  $E_{kl}$  is always at most  $\Im(\lambda_k^{\text{in}}) + \Im(\lambda_l^{\text{out}})$ , i.e., proportional to their combined energy.

We define the total error by finding a least-cost perfect matching of the bipartite graph with edge costs  $E_{kl}$ . Let  $l(k)$  denote a perfect matching, which assigns each input eigenvalue  $\lambda_k^{\text{in}}$  to the output eigenvalue  $\lambda_{l(k)}^{\text{out}}$  (see Fig. 3 and Fig. 4). The least-cost matching may be found in  $\mathcal{O}(M^3)$  time,  $M = \max(M^{\text{in}}, M^{\text{out}})$ , for example with fast versions of the Hungarian algorithm [27]. The final error is the cost of the least-cost perfect matching, normalized by the sum of imaginary parts of all eigenvalues at input and output:

$$E_{\text{ds}}(c_q) = \frac{\min_{l(k)} \sum_{k=1}^M E_{kl(k)}}{\sum_{k=1}^M \Im(\lambda_k^{\text{in}}) + \sum_{l=1}^M \Im(\lambda_l^{\text{out}})}, \quad (16)$$

in which  $M$ ,  $E_{kl}$ , and  $\lambda_m$  depend implicitly on  $c_q$ . In case no eigenvalues were found for both the input and output, we set  $E_{\text{ds}}$  to its maximum value, 1. We find an estimate  $\tilde{c}_q$  as the value minimizing  $E_{\text{ds}}(c_q)$ .

*Edge cost  $E_{kl}$ :* Next, we consider the edge cost  $E_{kl}$  to represent the mismatch  $E_{kl}$  between  $\lambda_k^{\text{in}}$  and  $\lambda_l^{\text{out}}$ . A straightforward, but effective edge cost  $E_{kl}$  is the Euclidean distance between input and output eigenvalue. However, with this norm, eigenvalue pairs with small imaginary part, but large difference in real part may dominate the error, whereas their energy ( $\propto$  imaginary part) can be arbitrarily small. To ensure that eigenvalue pairs with low energy cannot dominate the total error, we put an upper bound on  $E_{kl}$ , equal to the sum of the imaginary parts of the eigenvalue pair:

$$E_{kl} = \min(|\lambda_k^{\text{in}} - \lambda_l^{\text{out}}|, \Im(\lambda_k^{\text{in}}) + \Im(\lambda_l^{\text{out}})). \quad (17)$$

This way, if  $\lambda_k^{\text{in}}$  and  $\lambda_l^{\text{out}}$  contain little energy, they can also contribute little to the total error. A mathematical motivation for this upper bound for  $E_{kl}$  is that new eigenvalues may appear at the real axis as  $c_q$  is varied. Therefore, we can argue that instead of connecting an input and output eigenvalue to each other, it may also be the case that each connects to a hypothetical eigenvalue which is about to appear on the real axis right beneath it, resulting in an error of  $\Im(\lambda_k^{\text{in}}) + \Im(\lambda_l^{\text{out}})$ . Note that the connection between an eigenvalue  $\lambda_m$  and an auxiliary eigenvalues  $\lambda^{\text{aux}} = 0$  always assumes its maximum bound,  $\Im(\lambda_m)$ .

Although the edge cost in Eq. 17 suffices in most circumstances, an alternative definition for  $E_{kl}$  may be used when we already have a reliable estimate for  $Z$  available.  $Z$  may be available when  $\beta_2$  and  $L$  are already known, and only  $\gamma_1$  is to be identified, or when  $Z$  was reliably estimated by the continuous spectrum algorithm. If  $Z$  is available, we may define the error  $E_{kl}$  using both a mismatch in eigenvalue,  $E_{kl}^\lambda$ , as well as a mismatch in spectral function,  $E_{kl}^b$ , (opposed to only using the mismatch in  $\lambda$  as in (17)). Let the mismatch in eigenvalue be given by the Euclidean distance between the paired eigenvalues,

$$E_{kl}^\lambda := |\lambda_k^{\text{in}} - \lambda_l^{\text{out}}|. \quad (18)$$

Second, we consider the mismatch in the spectral function  $b$ . According to Eq. 9,  $b(\lambda, Z/T_0^2) = b(\lambda, 0)e^{4i\lambda^2 Z/T_0^2}$ . Let  $\lambda_{kl} :=$

$\frac{\lambda_k^{\text{in}} + \lambda_{l(k)}^{\text{out}}}{2}$  be the average of the input and output eigenvalue. We may express the difference between  $b_k^{\text{in}}$  and  $b_l^{\text{out}} e^{-4i\lambda_{kl}^2 Z/T_0^2}$  as the result of a difference  $\Delta\lambda$  in  $\lambda_{kl}$ :

$$\begin{aligned} b_k^{\text{in}} &= b_l^{\text{out}} e^{-4i(\lambda_{kl} + \Delta\lambda)^2 Z/T_0^2}, \\ \Rightarrow b_k^{\text{in}} &= b_l^{\text{out}} e^{-4i\lambda_{kl} Z/T_0^2 - 8i\lambda_{kl} \Delta\lambda Z/T_0^2 + \mathcal{O}(\Delta\lambda^2)}. \end{aligned}$$

By dropping the quadratic term  $\mathcal{O}(\Delta\lambda^2)$ , we get a simple expression for the mismatch  $\Delta\lambda$  in the spectral data:

$$|\Delta\lambda| \approx E_{kl}^b := \left| \frac{\log\left(b_l^{\text{out}} e^{-4i\lambda_{kl} Z/T_0^2} / b_k^{\text{in}}\right)}{8i\lambda_{kl} Z/T_0^2} \right|, \quad (19)$$

and note that this relationship requires knowledge of  $Z$ . We finally define the total mismatch as the average of both errors, and bound it by the imaginary value of the eigenvalue pair:

$$E_{kl} := \min\left(\frac{E_{kl}^\lambda + E_{kl}^b}{2}, \Im(\lambda_k^{\text{in}}) + \Im(\lambda_l^{\text{out}})\right). \quad (20)$$

When a reliable estimate for  $Z$  is available, using edge cost (20) generally results in better estimates  $\tilde{c}_q$  compared to using (17).

*Determine  $Z$  from  $b(\lambda_m)$ :* We can (re-)estimate  $Z$  by comparing the  $|b^{\text{in}}(\lambda_k)|$  with  $|b^{\text{out}}(\lambda_{l(k)})|$  using the identified  $\tilde{c}_q$  and assignment  $l(k)$ . The spectral function at input and output for  $\lambda_m$  are related through Eq. 9, from which estimates  $\tilde{Z}_k$  may be obtained as

$$\begin{aligned} |b(\lambda_m, Z/T_0^2)| &= |b(\lambda_m, 0)| e^{\Re(4i\lambda_m^2 Z/T_0^2)} \\ \Rightarrow \tilde{Z}_k &= T_0^2 \frac{\log|b^{\text{out}}(\lambda_{l(k)})| - \log|b^{\text{in}}(\lambda_k)|}{\Re(4i\lambda_{kl}^2)}, \quad (21) \end{aligned}$$

where  $\tilde{Z}_k$  is an estimate for  $Z$  from the  $k^{\text{th}}$  eigenvalue pair, and  $\lambda_{kl} := \frac{\lambda_k^{\text{in}} + \lambda_{l(k)}^{\text{out}}}{2}$  is the average of the paired input and output eigenvalue. To use the available data as well as possible, we consider all  $\tilde{Z}_k$  for a final estimate  $\tilde{Z}$ . First, all pairs with maximal distance,  $E_{kl} = \Im(\lambda_k^{\text{in}}) + \Im(\lambda_l^{\text{out}})$ , are discarded, as these eigenvalues are very distant from each other and are unlikely to be related. Second, we discard outliers, i.e., estimations more than two standard deviations away from the mean. Outliers are common, as almost purely imaginary eigenvalues lead to a small denominator in (21), yielding unstable estimations for  $Z$ . Third, as eigenvalues with large imaginary part contain more energy, we assign their associated estimates a larger weight,  $w_k = \Im(\lambda_{kl})$ . The final  $\tilde{Z}$  is the weighted average of the remaining estimates,  $\tilde{Z} = \sum_k w_k \tilde{Z}_k / \sum_k w_k$ .

#### IV. FINAL IDENTIFICATION ALGORITHM

In this section, we combine all previously described algorithms to create one final robust algorithm. From our experience with the continuous and discrete spectrum, we have found that the continuous spectrum algorithm usually yields better results for  $Z$ , while the discrete spectrum algorithm yields more reliable results for  $c_q$ . Therefore, we will first attempt to use the continuous spectrum to identify  $Z$ , and then the discrete spectrum to identify  $c_q$ . If  $Z$  is identified reliably from the continuous

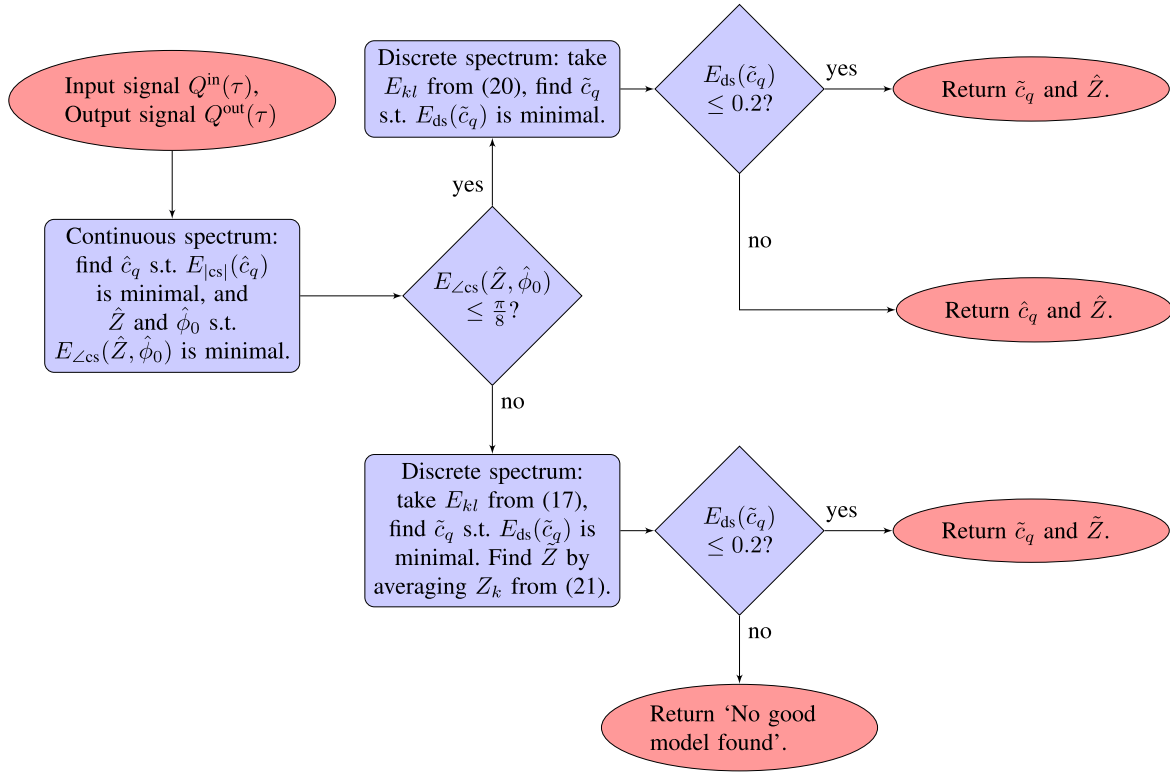


Fig. 5. Overview of the final algorithm.

spectrum, this  $Z$  may also be used for the discrete spectrum identification through Eq. 18–20.

In general, it holds that if the continuous or discrete spectrum contains too little energy, or the signal-to-noise ratio is too low, no good resemblance between input and output spectrum exists, and thus the estimates of the corresponding algorithm should be discarded. We therefore reject estimates for the continuous spectrum when  $E_{\angle cs} > \frac{\pi}{8}$  (average absolute phase mismatch) for the continuous spectrum algorithm, and  $E_{ds} > 0.2$  (relative error) for the discrete spectrum.

We propose a final algorithm as summarized in Fig. 5. First we find estimates  $\hat{c}_q$  and  $\hat{Z}$  using the continuous spectrum algorithm. If these estimates are accepted, we apply the discrete spectrum algorithm using the identified  $\hat{Z}$  to re-estimate  $c_q$ , and accept this estimate  $\tilde{c}_q$  if  $E_{ds} < 0.2$ . Otherwise, it is discarded. If the continuous spectrum algorithm estimates were rejected, we fully rely on the discrete spectrum algorithm. If the discrete spectrum error is sufficiently small,  $E_{ds} < 0.2$ , we accept the resulting estimates  $\tilde{c}_q$  and  $\tilde{Z}$ . In case both the continuous and discrete spectrum algorithm did not provide reliable results, we can enlarge our search range for the initial guess  $c_q^0$ . If this does not yield any reliable results either, the algorithm cannot identify a fitting normalization, most likely because the LPA-NLSE does not model the fiber well enough, or because the considered signal is too noisy. A more reliable estimate can be obtained by running the identification algorithm for multiple signals, discarding outlier estimates, and averaging over the remaining ones.

## V. RESULTS: IDENTIFICATION ON SIMULATED DATA

In this section, we demonstrate the capabilities of the identification algorithm on noisy transmission data simulated with Eq. 1. We have considered two applications: first, we identified the second-order dispersion  $\beta_2$ , and the Kerr nonlinearity coefficient  $\gamma$  using a conventional transceiver; second, without any prior knowledge, the algorithm was used to calibrate a nonlinear Fourier transform-based transmission system.

We applied the algorithm on input-output data from a fiber-optic transmission system, simulated with the software *NFDM-lab* [28]. For both applications, we considered the same NZ-DSF fiber link, with 20 spans of  $L_{\text{span}} = 80$  km each, resulting in a total transmission length of 1600 km. The second-order dispersion of the fiber was  $\beta_2 = -5.00 \cdot 10^{-27} \text{ s}^2 \text{ m}^{-1}$ , the Kerr nonlinearity coefficient was  $\gamma = 1.20 \cdot 10^{-3} \text{ (Wm)}^{-1}$ , and the attenuation coefficient was  $\alpha = 0.2 \cdot 10^{-3} \text{ dB/m}$ . After each span, an EDFA compensated the accumulated loss through lumped amplification, and added white Gaussian noise with a noise figure of  $f_n = 6$  dB. We used the LPA-NLSE (4) as reference solution, which predicted a path-averaged (PA) model with path-averaged Kerr nonlinearity coefficient  $\gamma_1 = 0.318 \cdot 10^{-3} \text{ (Wm)}^{-1}$ , normalization coefficient  $c_q = 2.52 \cdot 10^{11} \text{ W}^{-1/2} \text{ s}^{-1}$ , and normalized length  $Z = 4.00 \cdot 10^{-23} \text{ s}^2$ . At the link input and output, ideal low-pass filters were applied to account for transceiver bandwidth limitations [28]. We assume that all other real-world effects not included in the model are either zero-mean and can be included in the noise term, or that they have been removed by appropriate post-processing. For example, a carrier frequency

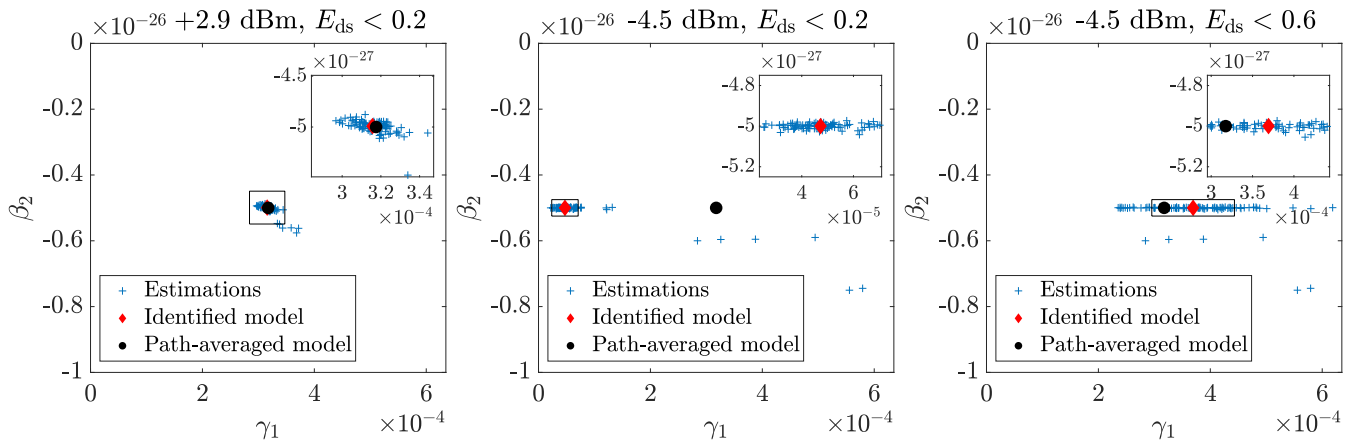


Fig. 6. The identified path-averaged Kerr nonlinearity and second-order dispersion from conventional transceiver data. Left: high launch power (2.9 dBm) and unadapted algorithm. Middle: medium launch power ( $-4.5$  dBm) and the unadapted algorithm (middle). Right: medium launch power ( $-4.5$  dBm), increased acceptance rate from  $E_{ds} < 0.2$  to  $E_{ds} < 0.6$  for the discrete algorithm part.

offset can be detected and compensated with a simple nonlinear-frequency shift [19]. We finally assume a coherent receiver since both phase and amplitude information are required. To compute the NFT in the identification algorithm, we used the *Fast Nonlinear Fourier Transform* (FNFT) software library [29].

#### A. Identifying Fiber Coefficients From a Conventional Transceiver

In this benchmark, we simulated data transmission using a conventional time domain transceiver, and show that the fiber coefficients  $\beta_2$  and  $\gamma$  can be accurately recovered. We assume that the fiber length, amplifier spacing, and attenuation coefficient are known. The transmitted signal consists of a linear sum of time-shifted raised cosine pulses, modulated with Quadrature Phase Shift Keying (QPSK). The roll-off factor was 0.5 and symbol duration  $T = 0.04$  ns. The time shift between two subsequent pulses is also  $T = 0.04$  ns, to ensure zero intersymbol interference (ISI) in the transmitted signal. The transmitted signal consisted of burst of 128 pulses. In between two bursts, a guard interval of  $16T$  was added. We considered two cases: one with optimal launch power,  $-4.5$  dBm, and one with high launch power, 2.9 dBm. The optimal launch power was found by optimizing detection performance after applying digital (linear) dispersion compensation and average rotation compensation of the symbols. Note that the NFT spectrum of this signal was not specially tailored, we only spaced the bursts sufficiently far apart with guard intervals such that the bursts did not significantly interfere at output, and could be analysed separately.

For both cases, we transmitted a signal with 100 bursts, and applied our algorithm to each burst at transmitter and receiver. The identified coefficients were determined by first discarding outliers (more than two standard deviations away from the mean), and then averaging over the remaining estimations. The path averaged coefficients were used as reference solution. First, we consider the result for the high power signal, which are shown on the left in Fig. 6. The identified coefficients were  $\beta_2 = -4.99 \cdot 10^{-27}$  s<sup>2</sup> m<sup>-1</sup> (PA:  $-5.00 \cdot 10^{-27}$ ) and  $\gamma_1 =$

$3.16 \cdot 10^{-4}$  (Wm)<sup>-1</sup> (PA:  $3.18 \cdot 10^{-4}$ ). The corresponding Kerr nonlinearity coefficient was  $\gamma = 1.19 \cdot 10^{-3}$  (Wm)<sup>-1</sup> (true:  $1.20 \cdot 10^{-3}$ ). Both coefficients were less than 1% off the true values, showing that the fiber coefficients can be accurately identified using our algorithm if the launch power is sufficiently high.

Next, we consider the case with optimal launch power. The algorithm still reliably identifies  $\beta_2$ , but the estimate of  $\gamma$  is poor. See the middle of Fig. 6. The poor performance of the algorithm with respect to  $\gamma$  is due to the fact that at optimal launch power (for a linear transceiver), nonlinear effects are insignificant compared to the dispersive effect over the considered fiber length. During further analysis, we observed that while the signals were actually dominated by solitonic components (about 80% of the total signal energy), the discrete spectrum was consistently rejected due to significant mismatch in  $b(\lambda_j)$  in Eq. 19. (Similar observations in which conventional OFDM signals were found to be soliton-dominated have been reported in [30]. Note that the solitons do not disentangle since the fiber is too short.) The current estimates were thus solely based on the continuous spectrum. In order to get a good estimate of the nonlinearity parameter  $\gamma$  at optimal transmit power (for a linear transceiver), we should not discard the discrete spectrum. Hence, we increased the acceptance rates for the discrete estimates from 0.2 to 0.6 (this corresponds to accepting the discrete estimates in almost all cases). The result is shown on the right in Fig. 6. The new estimate is much better than before, although it is still biased and the individual data points show a large variance. Thus, we were eventually able to obtain a reasonable estimate of the nonlinearity coefficient. However, the benchmark also shows that for highly accurate estimates of the nonlinearity parameter, the launch power has to be high enough such that nonlinear effects are not negligible.

#### B. Calibrating an NFT-Based Transceiver

In our second benchmark, we considered a scenario in which we modulated data in the discrete NFT-spectrum. If the correct

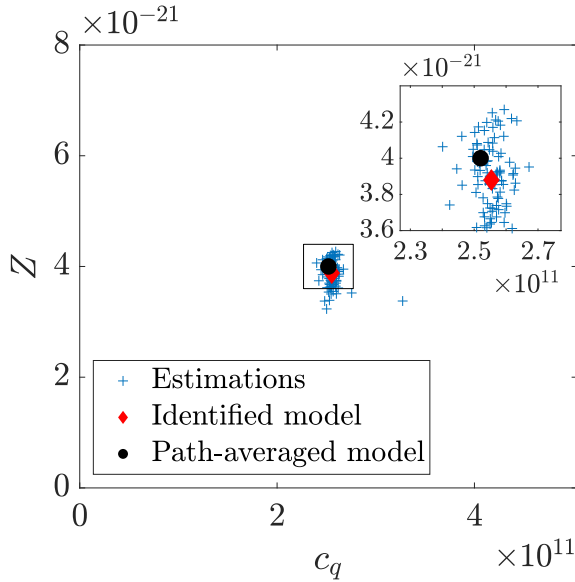


Fig. 7. The identified normalization from multi-soliton transceiver data. No prior knowledge of the fiber was used.

normalization was used for the modulation, the transmitted signal would consist of bursts of multi-solitons with 7 eigenvalues  $\lambda_m$  and zero continuous spectrum. Bits were modulated into the phase of the residues,  $\tilde{q}_m = b/a_\lambda(\lambda_m)$ , of each eigenvalue using QPSK, identically following the modulation format of Bülow *et al.* [26]:  $\angle(\tilde{q}(\lambda_m^{\text{in}})) \in \{-\frac{3\pi}{4}, -\frac{\pi}{4}, \frac{\pi}{4}, \frac{3\pi}{4}\}$ . The time normalization constant was  $T_0 = 2 \text{ ns}/(14\pi)$ , which transformed the bursts with normalized duration  $14\pi$  to bursts of physical duration 2 ns. We emphasize that it is no problem if the identification algorithm uses a different value for  $T_0$  when normalizing the input and output data. (When data is modulated in the normalized nonlinear Fourier domain and then transformed into the physical time-domain, the choice of the normalization parameter influences the physical duration and amplitude of the fiber input and thus has to be chosen correctly. In contrast, for the identification algorithm, physical data is the starting point and the time normalization constant only influences in which normalized domain the nonlinear spectra are compared. The only important point is that the input and output data have to be normalized using the same constant.)

Only the correct normalization  $c_q$  and the normalized length  $Z$  are required for successful transmission, but these were guessed poorly as  $c_q = 3.00 \cdot 10^{11} \text{ W}^{-1/2}\text{s}^{-1}$  (PA:  $2.52 \cdot 10^{11}$ ) and  $Z = 8.00 \cdot 10^{-23} \text{ s}^2$  (PA:  $4.00 \cdot 10^{-23}$ ). As a result, the error vector magnitude (EVM) in the received symbols was 35 dB, and communication was unsuccessful. Although the symbols could not be recovered, we could use the transmitted and received signals to identify a new model. We applied the combined algorithm to each of 100 bursts of presumed 7-soliton signals, discarded outlier estimates (more than 2 standard deviations away from the mean), and averaged the remaining estimates to obtain  $c_q = 2.54 \cdot 10^{11} \text{ W}^{-1/2}\text{s}^{-1}$  and  $Z = 3.85 \cdot 10^{-21} \text{ s}^2$ , as shown in Fig. 7. Using this new normalization, we generated a signal modulated with new symbols, and the symbols were successfully received. The transmission with the identified model resulted in

an EVM of  $-8.2$  dB in the symbols, whereas the path-averaged model resulted in  $-8.6$  dB. Thus the identified model performed comparable to the path-averaged model, only showing a minor increase in EVM.

## VI. CONCLUSION

We have proposed an algorithm to identify the second-order dispersion  $\beta_2$  and Kerr nonlinearity coefficient  $\gamma$  of an optical fiber, based on the nonlinear Fourier transform (NFT) of transmitted and received signals. The algorithm models the fiber with a lossless, path-averaged nonlinear Schrödinger equation, and identifies a normalization for the NFT such that the corresponding NFT spectrum of the transmitted and received signal match optimally to each other.  $\beta_2$  and  $\gamma$  are finally derived from the identified normalization, using the known fiber length, amplifier spacing, and attenuation coefficient. Although  $\beta_2$  and  $\gamma$  cannot be found without prior knowledge of the fiber, the normalization can nonetheless be identified, which already suffices to calibrate an NFT-based transceiver. The entire algorithm can be applied on any sufficiently high energy signal, and does not require special training signals.

We have demonstrated the capabilities of the algorithm with two benchmarks, in which the fiber coefficients were accurately identified. Due to its versatility and accuracy, the proposed identification algorithm may prove an attractive alternative to currently existing fiber identification methods.

## APPENDIX

### IDENTIFICATION FROM CONSERVED QUANTITIES

The normalized focusing NLSE (6) has an infinite number of conserved quantities [15], the first three of which are

$$C_1 = - \int_{-\infty}^{\infty} |q|^2 dt, \quad (22)$$

$$C_2 = \frac{1}{2} \int_{-\infty}^{\infty} qq_t^* - q^* q_t dt, \quad (23)$$

$$C_3 = \int_{-\infty}^{\infty} |q|^4 - |q_t|^2 dt. \quad (24)$$

The value of these constants does not depend on the location in the fiber as long as the signal propagates according to the NLSE. Given an arbitrary input signal  $q^{\text{in}}(t) = T_0 c_q Q^{\text{in}}(T_0 t)$  and its corresponding output signal  $q^{\text{out}}(t) = T_0 c_q Q^{\text{out}}(T_0 t)$ , we may determine  $c_q$  by comparing  $C_3$  at input and output:

$$\begin{aligned} C_3^{\text{in}}(c_q) &= C_3^{\text{out}}(c_q), \Rightarrow \int_{-\infty}^{\infty} |c_q Q^{\text{in}}|^4 - |c_q Q^{\text{in}}|^2 d\tau \\ &= \int_{-\infty}^{\infty} |c_q Q^{\text{out}}|^4 - |c_q Q^{\text{out}}|^2 d\tau, \\ &\Rightarrow c_q^2 = \frac{\int_{-\infty}^{\infty} |Q^{\text{in}}(\tau)|^2 - |Q^{\text{out}}(\tau)|^2 d\tau}{\int_{-\infty}^{\infty} |Q^{\text{in}}(\tau)|^4 - |Q^{\text{out}}(\tau)|^4 d\tau}. \end{aligned} \quad (25)$$

This relation provides a fast and easy method to obtain estimates for  $c_q > 0$ . We note that the first and second conserved quantities cannot be used in a similar fashion because  $c_q$  drops out when equating them. On the other hand, higher conserved quantities

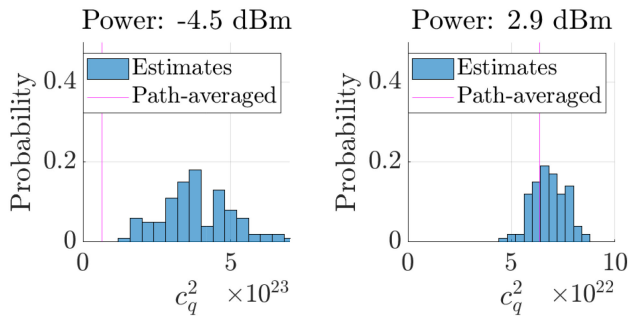


Fig. 8. The distribution of  $c_q^2$ , estimated from the conserved quantity  $C_3$  of a transmitted raised cosines signal at launch powers of  $-4.5$  dBm and  $2.9$  dBm. Note the difference in scale between the plots.

can be used, but contain higher derivatives and powers, which are increasingly sensitive to noise. Using  $C_3$  through Eq. 25 is thus the most suitable to estimate  $c_q$ . Using optimal linear launch power ( $-4.5$  dBm) and high-power ( $2.9$  dBm) signals from the conventional transceiver, described in Section VI, we have determined  $c_q^2$  from 100 bursts. The results are shown in Fig. 8. At  $-4.5$  dBm launch power, the estimates are highly biased, and the resulting  $c_q$  is a factor 2.5 too high (i.e.,  $c_q^2$  about 6 times too high). At higher launch power, the estimates for  $c_q$  improve, but still contain a bias of about 5%. In general, we observed that changing the modulation format or the fiber itself can drastically influence the bias. Furthermore, the estimates are very sensitive to noise, considered bandwidth and interference with neighboring bursts. The estimates are unfortunately too biased and unstable to immediately use as final estimates for  $c_q$ , but they still provide an order-of-magnitude indication, and can be used as initial estimates for our NFT-based identification algorithm.

#### ACKNOWLEDGMENT

The authors would like to thank the anonymous reviewers for their helpful comments, in particular, for the suggestion to consider conserved quantities.

#### REFERENCES

- [1] G. P. Agrawal, *Fiber-Optic Communication Systems*. Hoboken, NJ, USA: Wiley, 2012, vol. 222.
- [2] E. Agrell *et al.*, "Roadmap of optical communications," *J. Opt.*, vol. 18, no. 6, 2016, Art. no. 063002.
- [3] P. J. Winzer, D. T. Neilson, and A. R. Chraplyvy, "Fiber-optic transmission and networking: The previous 20 and the next 20 years," *Opt. Express*, vol. 26, no. 18, pp. 24 190–24 239, 2018.
- [4] P. de Koster and S. Wahls, "Fibre model identification for nonlinear Fourier transform-based transmission," in *Proc. IEEE 45th Eur. Conf. Opt. Commun.*, 2019, pp. 1–4.
- [5] F. N. Hauske, C. Xie, Z. Zhang, C. Li, L. Li, and Q. Xiong, "Frequency domain chromatic dispersion estimation," in *Proc. IEEE Conf. Opt. Fiber Commun. Collocated Nat. Fiber Optic Eng. Conf.*, 2010, pp. 1–3.
- [6] Q. Sui, A. P. T. Lau, and C. Lu, "Fast and robust blind chromatic dispersion estimation using auto-correlation of signal power waveform for digital coherent systems," *J. Lightw. Technol.*, vol. 31, no. 2, pp. 306–312, Jan. 2013.
- [7] C.-Y. Lin *et al.*, "Adaptive digital back-propagation for optical communication systems," in *Proc. Opt. Fiber Commun. Conf.*, 2014, Paper M3C.4.
- [8] M. Piels, E. P. da Silva, D. Zibar, and R. Borkowski, "Performance emulation and parameter estimation for nonlinear fibre-optic links," in *Proc. IEEE 21st Eur. Conf. Netw. Opt. Commun.*, 2016, pp. 1–5.
- [9] L. Prigent and J.-P. Hamaide, "Measurement of fiber nonlinear Kerr coefficient by four-wave mixing," *IEEE Photon. Technol. Lett.*, vol. 5, no. 9, pp. 1092–1095, Sep. 1993.
- [10] L. Jiang *et al.*, "Chromatic dispersion, nonlinear parameter, and modulation format monitoring based on Godard's error for coherent optical transmission systems," *IEEE Photon. J.*, vol. 10, no. 1, Feb. 2018, Art. no. 7900512.
- [11] Y. Namihira, A. Miyata, and N. Tanahashi, "Nonlinear coefficient measurements for dispersion shifted fibres using self-phase modulation method at  $1.55 \mu\text{m}$ ," *Electron. Lett.*, vol. 30, no. 14, pp. 1171–1172, 1994.
- [12] A. Boskovic, S. Chernikov, J. Taylor, L. G.-Nielsen, and O. Levring, "Direct continuous-wave measurement of  $n_2$  in various types of telecommunication fiber at  $1.55 \mu\text{m}$ ," *Opt. Lett.*, vol. 21, no. 24, pp. 1966–1968, 1996.
- [13] P. André and J. Pinto, "Simultaneous measurement of the nonlinear refractive index and chromatic dispersion of optical fibers by four-wave mixing," *Microw. Opt. Technol. Lett.*, vol. 34, no. 4, pp. 305–307, 2002.
- [14] A. Shabat and V. Zakharov, "Exact theory of two-dimensional self-focusing and one-dimensional self-modulation of waves in nonlinear media," *Sov. Phys. JETP*, vol. 34, no. 1, pp. 62–69, 1972.
- [15] M. J. Ablowitz, D. J. Kaup, A. C. Newell, and H. Segur, "The inverse scattering transform-Fourier analysis for nonlinear problems," *Studies Appl. Math.*, vol. 53, no. 4, pp. 249–315, 1974.
- [16] S. K. Turitsyn *et al.*, "Nonlinear Fourier transform for optical data processing and transmission: Advances and perspectives," *Optica*, vol. 4, no. 3, pp. 307–322, 2017.
- [17] S. T. Le, J. E. Prilepsky, and S. K. Turitsyn, "Nonlinear inverse synthesis technique for optical links with lumped amplification," *Opt. Express*, vol. 23, no. 7, pp. 8317–8328, 2015.
- [18] M. I. Yousefi and F. R. Kschischang, "Information transmission using the nonlinear Fourier transform, Part III: Spectrum modulation," *IEEE Trans. Inf. Theory*, vol. 60, no. 7, pp. 4346–4369, Jul. 2014.
- [19] M. I. Yousefi and F. R. Kschischang, "Information transmission using the nonlinear Fourier transform, Part I: Mathematical tools," *IEEE Trans. Inf. Theory*, vol. 60, no. 7, pp. 4312–4328, Jul. 2014.
- [20] X. Yangzhang, V. Aref, S. T. Le, H. Bülow, and P. Bayvel, "400 Gbps dual-polarisation non-linear frequency-division multiplexed transmission with b-modulation," in *Proc. IEEE Eur. Conf. Opt. Commun.*, 2018, pp. 1–3.
- [21] J. C. Lagarias, J. A. Reeds, M. H. Wright, and P. E. Wright, "Convergence properties of the Nelder–Mead simplex method in low dimensions," *SIAM J. Optim.*, vol. 9, no. 1, pp. 112–147, 1998.
- [22] J. Satsuma and N. Yajima, "B. Initial value problems of one-dimensional self-modulation of nonlinear waves in dispersive media," *Prog. Theoretical Phys. Suppl.*, vol. 55, pp. 284–306, 1974.
- [23] E. Fagerstrom, "On the nonlinear Schrödinger equation with nonzero boundary conditions," Ph.D. dissertation, Dept. Math., Univ. Buffalo, State Univ. New York, Buffalo, NY, USA, 2015.
- [24] M. Klaus and J. Shaw, "On the eigenvalues of Zakharov–Shabat systems," *SIAM J. Math. Anal.*, vol. 34, no. 4, pp. 759–773, 2003.
- [25] A. Hasegawa and Y. Kodama, "Guiding-center soliton in optical fibers," *Opt. Lett.*, vol. 15, no. 24, pp. 1443–1445, 1990.
- [26] H. Bülow, V. Aref, and W. Idler, "Transmission of waveforms determined by 7 eigenvalues with PSK-modulated spectral amplitudes," in *Proc. 42nd Eur. Conf. Opt. Commun.*, 2016, pp. 1–3.
- [27] H. W. Kuhn, "The Hungarian method for the assignment problem," *Naval Res. Logistics Quart.*, vol. 2, no. 1-2, pp. 83–97, 1955.
- [28] M. Brehler, C. Mahnke, S. Chimmalgi, and S. Wahls, "NFDMLab: Simulating nonlinear frequency division multiplexing in Python," in *Proc. Opt. Fiber Commun. Conf.*, 2019, Paper M3Z.13.
- [29] S. Wahls and H. V. Poor, "Fast numerical nonlinear Fourier transforms," *IEEE Trans. Inf. Theory*, vol. 61, no. 12, pp. 6957–6974, Dec. 2015.
- [30] S. K. Turitsyn, E. Sedov, A. Redyuk, and M. P. Fedoruk, "Nonlinear spectrum of conventional OFDM and WDM return-to-zero signals in nonlinear channel," *J. Lightw. Technol.*, vol. 38, no. 2, pp. 352–358, Jan. 2020.